












Cite this: *Nanoscale*, 2019, **11**, 19468

Temperature-induced molecular reorganization on Au(111) driven by oligomeric defects†

F. De Marchi, ^{‡a} G. Galeotti, ^{‡a,b} M. Simenas, ^c M. C. Gallagher, ^{*d}
E. Hamzehpoor, ^e O. MacLean, ^a R. M. Rao,^e Y. Chen,^e D. Dettmann, ^b
G. Contini, ^{b,f} E. E. Tornau,^g M. Ebrahimi, ^{*§a} D. F. Perepichka ^{*e} and F. Rosei ^{*a}

The formation of ordered molecular structures on surfaces is determined by the balance between molecule–molecule and molecule–substrate interactions. Whether the aggregation process is guided by non-covalent forces or on-surface reactions, a deeper understanding of these interactions is pivotal to formulating *a priori* predictions of the final structural features and the development of bottom-up fabrication protocols. Theoretical models of molecular systems corroborate the information gathered through experimental observations and help explain the thermodynamic factors that underpin on-surface phase transitions. Here, we report a scanning tunneling microscopy investigation of a tribromo-substituted heterotriangulene on the Au(111) surface, which initially forms an extended close-packed ordered structure stabilized by Br...Br halogen bonds when deposited at room temperature. X-ray photoelectron spectroscopy reveals that annealing the self-assembled layer induces a fraction of the molecular precursors to partially dehalogenate that in turn leads to the formation of a less stable Br...O non-covalent network which coexists with the short oligomers. Density functional theory (DFT) and Monte Carlo (MC) simulations illustrate how dimer moieties act as defects whose steric hindrance prevents the retention of the more stable configuration. A small number of dimers is sufficient to drive the molecular reorganization into a lower cohesive energy phase. Our study shows the importance of a combined DFT – MC approach to understand the evolution of molecular systems on substrates.

Received 18th July 2019,
Accepted 6th September 2019

DOI: 10.1039/c9nr06117g

rsc.li/nanoscale

Introduction

Molecular self-assembly is one of the most important nanoscale phenomena.¹ It is the fundamental principle which life as it is known is based on. It has been studied and replicated

as a fabrication approach, starting from single molecules *via* the so called bottom-up approach.² The possibility of steering molecular self-assembly on surfaces would open interesting opportunities to be exploited in technological applications.^{3,4} The *a priori* design of 2D self-assembly relies primarily on understanding the driving forces that characterize the molecular building blocks, often dependent on specific functional groups, which can then be used for bottom-up fabrication in areas such as nanoelectronics,⁵ sensing,⁶ catalysis⁷ and energy storage among others.⁸ The formation of such complex surface patterns at the molecular scale relies on the self-assembly of organic functional molecules on solid substrates, driven by an intricate equilibrium between molecule–molecule and molecule–substrate interactions.^{2,9} Controlling such processes is a significant challenge, that needs to be tackled by building up a rigorous experimental database and by developing suitable theoretical techniques, to understand the experimental data, the forces at play, and the evolution of the system. Such an effort is necessary to combine the rational design of precursors with the prediction of their behavior and properties.

Despite the importance of developing a formal understanding of self-assembly on surfaces, only a few examples in the literature have tried to create a comprehensive model *a priori*

^aCentre Énergie, Matériaux et Télécommunications, Institut National de la Recherche Scientifique, 1650 Boulevard Lionel-Boulet, Varennes, Québec, Canada J3X 1S2.

E-mail: rosei@emt.inrs.ca

^bIstituto di Struttura della Materia, CNR, Via Fosso del Cavaliere 100, 00133 Roma, Italy

^cFaculty of Physics, Vilnius University, Saulėtekio 9, LT-10222 Vilnius, Lithuania

^dDepartment of Physics, Lakehead University, 955 Oliver Rd, Thunder Bay, Ontario, Canada P7B 5E1. E-mail: mcgallag@lakeheadu.ca, mebrahim@lakeheadu.ca

^eDepartment of Chemistry, McGill University, 801 Sherbrooke Street West, Montreal, Québec, Canada H3A 0B8. E-mail: dmitrii.perepichka@mcgill.ca

^fDepartment of Physics, University of Rome Tor Vergata, Via della Ricerca Scientifica 1, 00133 Roma, Italy

^gSemiconductor Physics Institute, Center for Physical Sciences and Technology, Saulėtekio 3, LT-10222 Vilnius, Lithuania

†Electronic supplementary information (ESI) available. See DOI: 10.1039/c9nr06117g

‡These authors contributed equally.

§Present address: Department of Chemistry, Lakehead University, 955 Oliver Road Thunder Bay, Ontario, Canada P7B 5E1.

describe the arrangement of the self-assembly,^{10,11} and thus allow the analytical design of the building blocks. Specifically, an extensive theory on the influence of the key parameters, such as temperature,¹² coverage/concentration of the monomers,¹³ or the polymorphism of the self-assembled monolayers (SAM) is lacking.^{14,15}

A plethora of different molecular interactions can be used to guide the formation of self-assembled molecular networks (SAMN), with common examples being van der Waals,¹⁶ hydrogen bonding¹⁷ and π - π stacking.¹⁸ An interesting class of interaction is represented by halogen bonds,¹⁹ which generate stable 2D geometric structures.^{15,20,21} The main feature of the halogen bond is the double polarization of the carbon-halogen (C-X) bond, where the bond is positively charged on the halogen (σ -hole), while around it a negative ring-like charge distribution is observed (belt).^{20,22} This peculiarity allows the halogen to interact with multiple atoms, forming patterns whose geometry is defined by the shape of the charge distribution.²⁰ This shape, and hence the interaction strength, can be modified by changing the halogen, with a more positive σ -hole for heavier atoms.²³

In addition to being building blocks for the formation of SAMNs, halogen-terminated molecules can be activated by a metallic surface to undergo Ullmann coupling. On surface Ullmann coupling of halogenated aromatic precursors is the most studied bottom-up approach for the synthesis of two-dimensional (2D) conjugated polymers.^{24,25} Ideally, the process follows a two-step procedure, with halogenated molecules initially deposited onto a metal substrate, where they diffuse to form an ordered structure stabilized by non-covalent intermolecular interactions.^{24,26,27} Annealing the SAMNs allows the carbon-halogen bonds to break and form organo-metallic structures with the substrate or polymeric structures if the temperature is sufficiently high. Previous studies have helped untangle the different factors affecting the reaction, including the surface, the type of halogen, and the temperature.^{28,29} This has made it possible to devise strategies to greatly improve the architecture of the reaction products,^{30–32} but the realization of large-domain ordered conjugated polymers remains an open challenge.³³ Further improvements will require greater insight into the evolution of molecular organization throughout the reaction process.

We present the combined use of density functional theory (DFT) and Monte Carlo (MC) simulations to replicate and understand the experimental results of the adsorption of a tri-bromo-substituted heterotriangulene, 2,6,10-tribromo-4,8,12-trioxa-3a²-azadibenzo[*cd,mn*]pyrene (TBTANG, Fig. 1f) on the Au(111) surface. This molecule can also be considered as a brominated oxygen-bridged triphenylamine, where the three oxygen bridges help planarize the molecule and therefore improve the self-assembly relative to other triphenylamine systems. The Au(111) surface was chosen as substrate because of its low reactivity, which allows the molecule to remain intact upon adsorption and enables the dehalogenation process to be followed with a combination of scanning tunneling microscopy (STM) and X-ray photoelectron spectroscopy (XPS).²⁷ The $\sqrt{3} \times 22$ herringbone reconstruction of Au(111) is

a helpful marker to identify possible interactions between the substrate and molecules, and this reconstruction is often removed by the presence of halogen radicals.³⁴ We observed that TBTANG forms long-range ordered domains of molecules held together by halogen-halogen interactions when deposited onto Au(111) at room temperature (RT). The dehalogenation reaction is triggered by annealing, leading directly to the formation of short oligomers. STM reveals that incomplete polymerization triggers a phase change in the self-assembled networks, so as to better accommodate the oligomers formed.

Our study demonstrates how combined DFT-MC calculations can explain the phase transition caused by partial polymerization, and how such an approach could be applied to provide an *a priori* prediction of the arrangement of molecules during Ullmann reaction and contribute to solving the challenge of extending the order of two-dimensional structures to device-suitable scales.

Results and discussion

Deposition of TBTANG onto Au(111), held at RT, yields extended domains of SAMNs consisting of close-packed TBTANG molecules that follow the herringbone reconstruction of the substrate (Fig. 1a). STM images reveal individual molecular features with a triangular shape. In particular, we observe three bright spots in the central region of the molecule and another three at the molecular vertices (Fig. 1b). The molecule appears intact, inferred by the 1 nm side of the triangular molecular feature, obtained by line profiling of the STM images (Fig. S1†), which agrees with the Br-Br intramolecular distance of 1.05 nm calculated by DFT. Based on the symmetry of the molecule, we can assign the spots at the vertices to Br atoms, while the high contrast at the center of the molecules corresponds to the phenyl rings rather than to the oxygen bridge sites. This observation is in contrast to previous studies of related heterotriangulene molecules, in which bright central spots were observed for similar biases at the dimethyl or carbonyl groups bridge sites.^{35–37}

The unit cell of the SAMN is formed by two molecules and has dimensions of 1.5 ± 0.1 nm by 1.9 ± 0.1 nm and an angle of $117 \pm 3^\circ$ (Fig. 1b, azure box). The STM images suggest that adjacent molecules form six-halogen clusters (green dots in Fig. 1b) and interact through non-covalent halogen-halogen interactions. This molecular configuration positions the tip of each C-Br bond (which is positively charged) towards the negatively charged belt of the surrounding Br atoms.^{20–22} The multiple interactions possible with C-X bonds are reflected by the calculated electrostatic potential (ESP) maps (Fig. S4a†), which show Br...Br and Br...H interactions. We therefore denote this SAMN as the Br...Br phase.

Such an arrangement is similar to the ones studied by Gatti *et al.* for Br-terminated, threefold-symmetric triazine molecules at the phenyloctane/Au(111) interface.¹⁵ In contrast to their data, we do not observe any difference in the self-assembly between the fcc- and hcp-stacked regions,¹⁵ suggesting a

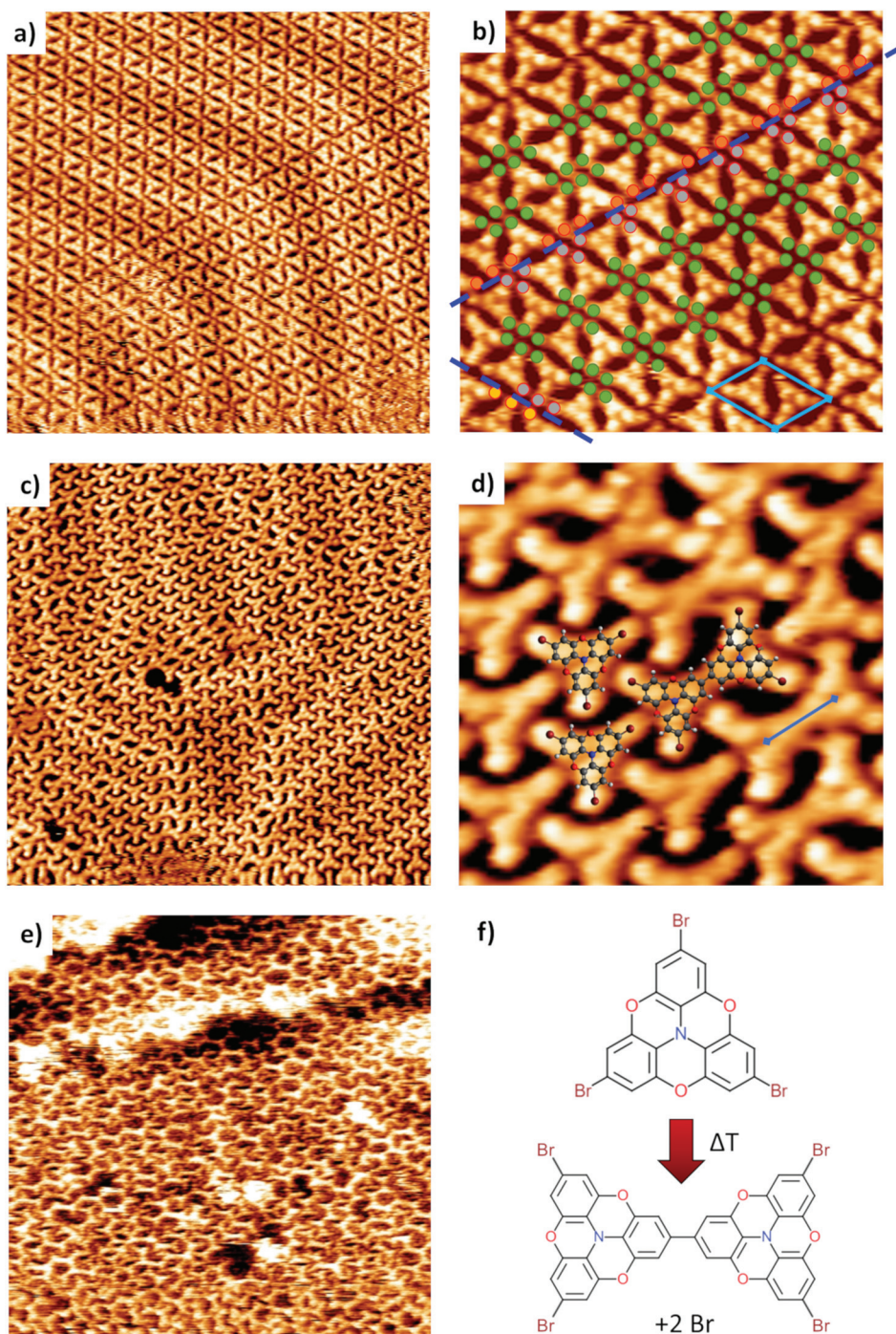


Fig. 1 (a) $25 \times 25 \text{ nm}^2$ STM image of TBtang dosed on Au(111) at RT ($I_t = 0.16 \text{ nA}$, $V_b = 0.39 \text{ V}$). (b) $10 \times 10 \text{ nm}^2$ detail of the RT phase in a, the blue lines indicate domains boundaries, while the colored dots represent the halogen packing, in green when in the ideal configuration and in different colors when on a stacking fault. (c) $25 \times 25 \text{ nm}^2$ STM images of TBtang dosed on Au(111) at RT and annealed at 150°C ($I_t = -1.25 \text{ nA}$, $V_b = -0.28 \text{ V}$). (d) $5 \times 5 \text{ nm}^2$. Detail of c, showing the presence of short oligomers ($I_t = -1.22 \text{ nA}$, $V_b = -0.28 \text{ V}$). (e) $25 \times 25 \text{ nm}^2$ STM images of TBtang dosed on Au(111) at RT and annealed at 250°C ($I_t = 1.33 \text{ nA}$, $V_b = 0.79 \text{ V}$). (f) structure for TBtang and the corresponding dimer.

weaker molecule...substrate interaction in our case. On the other hand, we observed stacking faults in the TBtang network located at the elbow of the herringbone pattern (blue lines in Fig. 1b), which results in a 60° rotation of the molecular unit cell for two adjacent domains.

Annealing the RT phase at 150°C for 20 minutes produces a less-ordered film (Fig. 1c). Most of the molecules remain intact, however some short oligomers (mostly dimers) are formed (Fig. 1c and d). STM reveals that the intact molecules still form a close-packed phase with the same three bright

spots at the molecular vertices previously assigned to Br atoms. At the border of the domains, adjacent molecules appear to be in close proximity (Fig. 1d). STM line profiles of these “closely-spaced” molecules exhibit a center-to-center distance of 0.97 ± 0.1 nm (Fig. S2†), which is consistent with TBTANG dimerization *via* C–C covalent linkage, as shown in Fig. 1d in which a molecular dimer has been superimposed on the image.

The remaining intact molecules in the self-assembled domains exhibit a different orientation than in the RT halogen-bonded phase, in which their vertices are directed towards the oxygen-bridge sites of the adjacent molecules (Fig. 1c and d). The unit cell dimensions are 1.2 ± 0.1 nm for both vectors with an angle of $122 \pm 3^\circ$. This SAMN is denoted as the Br...O phase, since the ESP maps indicate that the interaction is between the positively-charged σ -hole of the Br and the negatively-charged oxygen (Fig. S4b†). This agrees with the observation of Steiner *et al.* for similar heterotriangulene molecules,³⁶ where polymeric chains stabilized by Br...O intra-chains interactions were observed.

Further annealing of the as-grown SAMN at 250 °C for 20 minutes leads to drastic changes in molecular arrangement, as shown in Fig. 1e. The long-range ordered structure obtained at RT has disappeared, and the molecular overlayer consists of short molecular chains (mostly 3 to 5 molecular units), which in a few cases form closed hexagonal pore structures. The degree of order of the resultant layer is unaffected by the heating rate during annealing; in all the performed experiments only disordered polymers were obtained.

The STM data are supported by XPS spectra, which confirms that the molecule is still intact after adsorption on the Au(111) surface (Fig. 2a). In the C 1s spectra, the peaks at binding energies (BE) of 284.7 eV, 286.3 eV and 286.9 eV are attributed to C–C, C–O–C and C–N bonds, respectively.³⁸ The assignment of the 285.7 eV component as C–Br is based on a comparison with similar Br-terminated molecules studied on Ag(111) and Au(111), where the C–Br contribution was found at corresponding energies.^{27,39} XPS analysis of TBTANG SAMNs shows single O 1s and N 1s peaks at 533.6 and 400.2 eV, respectively (Fig. S3†). The Br 3p $3/2$ peak at 183.5 eV further confirms that the C–Br bonds are still intact and not broken upon adsorption (Fig. S3†).²⁷

To better understand the annealing process and to clarify the reason behind the loss of long-range ordering we acquired XPS spectra, reported in Fig. 2b, c and Fig. S3,† following the polymerization process at different temperatures. Annealing at 150 °C marks the onset of dehalogenation, with a reduction of the C–Br component, a shift of all the peaks to lower BE (see Fig. S3†) and a variation in the intensity ratio of C 1s double peak feature. The progressive oligomer formation is highlighted by the C 1s spectra at 250 °C, which shows an increase of the C–C component at the expense of the C–Br peak as the TBTANG further dehalogenates to form covalent bonds. After the initial significant shifts, the N 1s and O 1s peak shape and position remain stable through the polymerization process. Since only a small fraction of the molecules are dehalogenated

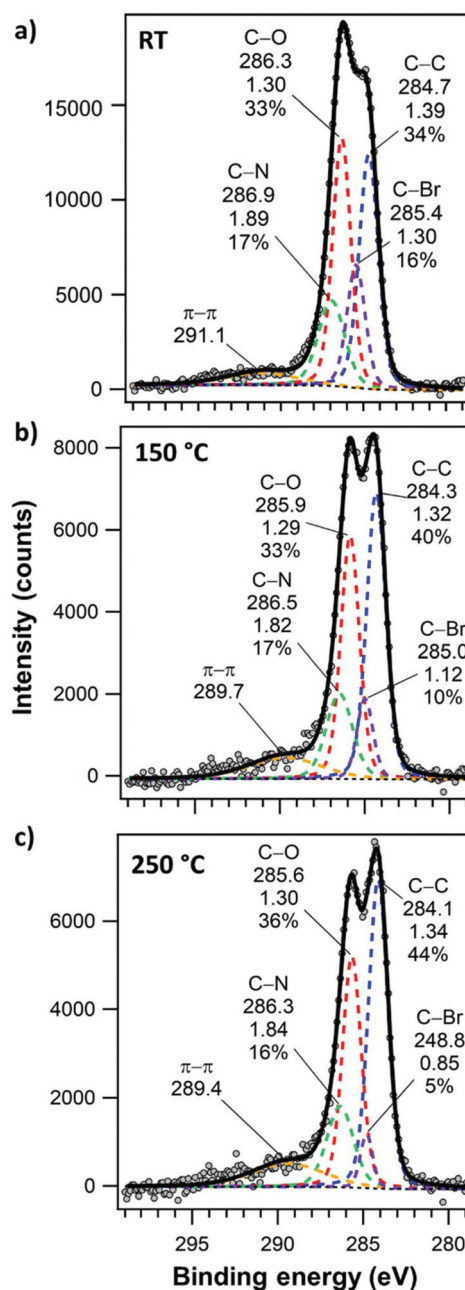


Fig. 2 XPS C 1s spectra of TBTANG/Au(111) at RT (a), 150 °C (b) and 250 °C (c). The BE peak position, full width at half maximum and intensity percentage are reported in each panel for every component.

at 150 °C, this shift is not caused by polymerization. Instead, it probably arises from the development of Br...O intermolecular interactions and a change in the molecular adsorption site in the modified SAMN.

The reduction in the C–Br component is coupled by a slight rise of the Br–Au component in the Br 3p spectra (Fig. S3b†). The small increase in the intensity of this Br–Au peak indicates that bromine atoms mainly desorb from the surface rather than remaining bound, which is probably due to a lack of available space on the surface considering the density of the

TBTANG SAMN at RT ($0.69 \text{ molec per nm}^2$). This is supported by the survival of the herringbone reconstruction after the initial dehalogenation (Fig. 1c and d), which is known to be lifted by the presence of adsorbed halogen atoms.^{34,40–42}

The SAMN structure is driven by molecule–molecule and molecule–substrate interactions, and it is not unusual to observe multiple phases with similar cohesive energies for a given molecule and substrate.^{14,43} Phase transitions observed after annealing are also common, and DFT calculations of the energies involved can help unravel the driving forces behind the transition.

We studied both of the observed SAMN phases by calculating the gas-phase assembly using DFT with periodic boundary conditions (Fig. 3). This allowed us to evaluate the Br...Br distances for the RT phase, finding an average of 0.39 nm , confirming halogen-bond phase stabilization. The two-molecule unit cell allows for six halogen packing, with a cohesive energy of $9.30 \text{ kcal per mol per molecule}$ (Fig. 3a). The DFT simulation of the annealed phase at 150°C shows that the C–Br tip is stabilized by the oxygen-bridges, and yields a cohesive energy of $8.83 \text{ kcal per mol per molecule}$ (Fig. 3b).

Comparing the two different self-assembled networks observed at RT and after annealing to 150°C , we find the same surface molecular density ($0.69 \text{ molecule per nm}^2$), but the DFT calculations reveal that the Br...Br phase obtained at RT is more stable by $0.47 \text{ kcal mol}^{-1}$ (per molecule) than the Br...O annealed phase. This energy difference computed in the gas-phase is consistent with the experimental observation of only the Br...Br phase after dosing at RT and with the ratio of interaction energies used in the Monte Carlo simulations (see below). We hypothesize that the Br...O configuration in the annealed films is favored because it can more easily accommodate TBTANG dimers or trimers, as the STM images (Fig. 1c and d) show close-packing between oligomer chains and Br...O stabilized molecules.

To test this hypothesis, we constructed a phase transition model of TBTANG ordering and monitored the evolution of the molecular system by MC simulations with an increasing

fraction of dimer pairs. Similar models are frequently used to describe the planar self-assembly of trimesic acid and other triangular molecules,⁴⁴ and MC simulations have been successfully applied to gain insight into the formation of 2D networks *via* Ullmann coupling.^{30,32}

At first, we studied the self-assembly of intact molecules, defining the possible configurations and interactions between single TBTANG units. As shown by Fig. 4a, our model includes two states of the intact molecules, which differ by a 60° rotation, and two intermolecular pair interactions, denoted e_1 and e_2 . Interaction e_1 occurs between molecules in different states and e_2 between molecules in the same state. The distance of the two TBTANG molecules participating in these interactions on a triangular lattice is $\sqrt{7}a$ (e_1) and $3a$ (e_2), where a is the lattice constant of the model. With such intermolecular distances, the molecules can be arranged into structures that closely resemble the experimentally observed Br...Br and Br...O phases respectively (Fig. 4b). The densities of both phases in our model are similar (0.128 and 0.111 mol/a^2) which agrees with the experimental observation of indistinguishable densities for the two phases. Our model forbids the overlap of molecules. Each molecule participates in three e_1 interactions in the Br...Br phase and six e_2 interactions in the Br...O phase. Thus, in the absence of other interactions and at zero temperature, the transition point between the two phases would occur at $e_2 = 0.5e_1$.

As revealed by Gaussian DFT calculations, the e_1 and e_2 interactions are the primary interactions driving the self-assembly into the Br...Br and Br...O phases (see ESI†). Other intermolecular interactions are much smaller and therefore not considered in our model. DFT calculations provide $e_1 = -5.69 \text{ kcal mol}^{-1}$ and $e_2 = -2.89 \text{ kcal mol}^{-1}$ and thus $e_2 \approx 0.5e_1$, which means that both phases in our model should have very similar energies in agreement with the plane-wave DFT calculations.

Next, we introduced dimers, formed by C–C coupling at higher temperatures, into our model to evaluate their influence on the self-assembly process. In our model, the dimers

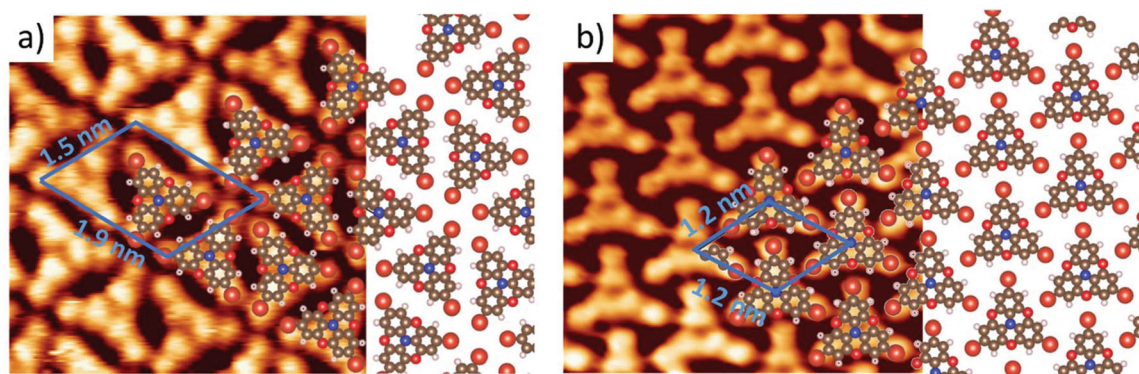


Fig. 3 $4 \times 4 \text{ nm}^2$ STM images of self-assembly for TBTANG on Au(111), at RT (a, $I_t = 0.16 \text{ nA}$, $V_b = 0.39 \text{ V}$) and after annealing the surface to 150°C (b, $I_t = -1.25 \text{ nA}$, $V_b = -0.28 \text{ V}$). Superimposed are the calculated gas phase DFT structures. Br...Br packing is $0.47 \text{ kcal mol}^{-1}$ more stable than Br...O packing. ($-9.30 \text{ kcal mol}^{-1}$ vs. $-8.83 \text{ kcal mol}^{-1}$ per molecule).

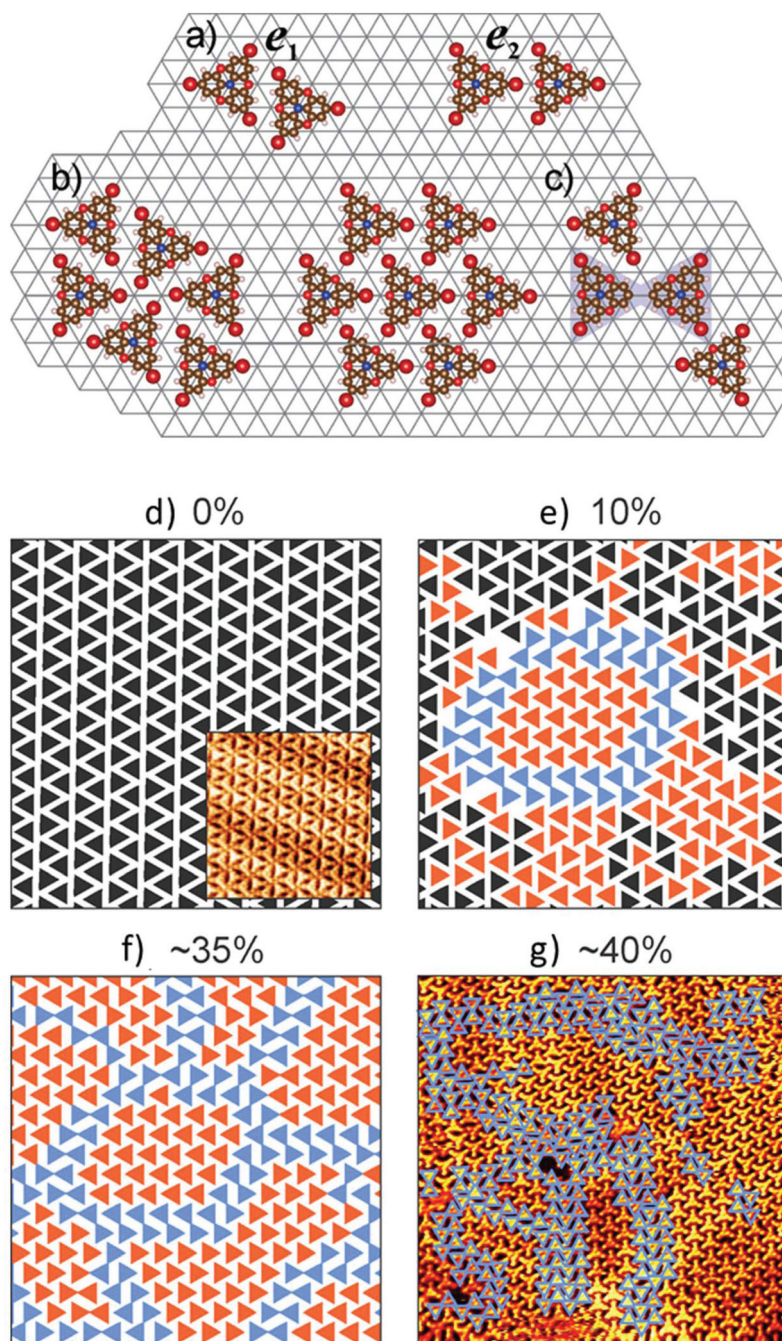


Fig. 4 (a) Model interactions e_1 and e_2 between two TBtang molecules used for MC simulations. (b) Fragments of molecular arrangements of the Br...Br and Br...O phases obtained in our model. (c) Example of e_1 and e_2 interactions between a dimer (shaded blue) and TBtang molecules. The triangular lattice used for MC simulations is presented in the background. (d–g) Structures of TBtang molecules as a function of the number of dimers obtained by the MC simulations. (d) 0% dimers: the Br...Br phase, experimental STM image presented in the inset. (e) 10% dimers (blue), the Br...O phase dominates inside the regions surrounded by the dimers, but the Br...Br structure is still present further from the dimers. (f) with about 35% dimers, only the Br...O structure is observed. Orange molecules have at least one e_2 interaction. (g) Experimental STM image with about 40% of oligomerized TBtang molecules. Interaction parameters: $e_2/e_1 = 0.48$.

are formed by joining TBtang molecules with overlapping vertices (distance between molecules 3a), and are artificially introduced onto the lattice to resemble the dimer chains observed by the STM. The same e_1 and e_2 interactions apply between individual TBtang molecules and the dimers (Fig. 4c).

In Fig. 4d–f we present our calculations with an increasing proportion of dimers using $e_2/e_1 = 0.48$ (very close to the DFT results) where in the absence of dimers, a pure Br...Br phase is obtained (Fig. 4d). A slight increase in the number of molecules forming dimers (10% of the total number of molecules)

leads to the formation of the Br...O phase inside islands surrounded by dimer chains (Fig. 4e). Motifs of the Br...O phase are also observed outside the dimer chains, while the structure further from the dimers corresponds to domains of the Br...Br phase with some occurrences of the e_2 interaction. An even further increase of dimers (35%) results in the formation of pure Br...O phase domains, in agreement with the experimental results (compare Fig. 4f and g).

Our MC results indicate that the formation of the Br...O phase is driven by the presence of dimers which are better accommodated by this phase. Although the e_2 interaction is weaker than e_1 , the greater number of e_2 interactions with dimers possible in the Br...O phase makes this configuration more stable overall. We determined that the Br...O phase can be observed for e_2/e_1 values down to about 0.45. Our MC simulations demonstrate the advantages of this approach to complement DFT calculations, enabling the study of the effects of reaction products or defects on self-assembly as well as providing a benchmark for the range of reasonable interaction energies.

Conclusions and perspectives

We have investigated the adsorption of a halogenated molecule, TBTANG, on the Au(111) surface. Dosing at RT leads to the self-assembly of intact molecules, which form close-packed extended networks, stabilized by Br...Br interactions. The long-range order of the self-assembled network is lost upon thermal annealing, which triggers molecular dehalogenation and ultimately the formation of disordered oligomer chains.

We followed the progressive drive towards disorder and found that the initial appearance of dimers and trimers triggers a phase transition in the remainder of the intact TBTANG molecules. The resultant phase has the same molecular density but is stabilized by Br...O interactions. DFT modeling does not explain the transition, as it reveals that the pure Br...Br packing is more stable than the Br...O phase by 0.47 kcal mol⁻¹ per molecule. Monte Carlo simulations of the mixed monomer-dimer system reveal that the oligomer density induces the phase transition and indicates that the two phases can coexist at intermediate values. Demonstrated collectively by our STM, XPS, DFT, and MC data, this study illustrates the on-surface molecular phase transition of self-assembled structures, offering insights into the mechanisms of the process, and the necessity of studying on-surface interactions between different functional groups to develop an *a priori* prediction of the resultant structures.

Experimental methods

The TBTANG precursor was synthesized according to the literature procedure.⁴⁵ All experiments were performed under ultrahigh vacuum (UHV) conditions with base pressures below 2×10^{-10} mbar. The Au(111) crystal was cleaned by repeated

cycles of Ar ion sputtering (1.0 keV for 10 minutes) and annealing (450 °C for 30 minutes). TBTANG was sublimed onto Au (111), held at RT, from a Knudsen cell (using an alumina crucible) at 120 °C to obtain a molecular coverage of a complete monolayer.

STM data were recorded using two commercial instruments (VT STM by Omicron GmbH and an Aarhus 150 STM by SPECS GmbH) using etched tungsten tips. STM images were calibrated using the known Au $\sqrt{3} \times 22$ surface reconstruction with the free WSxM software.⁴⁶ Further image processing included plane subtraction and flattening.

XPS experiments were performed *in situ* using an electron spectrometer (SPHERA II U5 analyzer by Oxford Instruments Omicron Nanoscience). The electron spectrometer consists of a hemispherical analyzer and a five-channeltron detector, with a twin-anode X-ray source using Mg K α radiation at 1254.6 eV photon energy. The spectra were analyzed with the CasaXPS software, using Voigt lineshape peaks and Shirley backgrounds, and the BE scale has been calibrated using the Au 4f_{7/2} peak at 84.00 eV.

Theoretical methods

Plane-wave theoretical calculations were performed for the extended SAMN phases using the Vienna *Ab initio* Simulation Package (VASP).^{47,48} DFT calculations were made using the Perdew–Burke–Ernzerhof⁴⁹ generalized-gradient approximation (PBE-GGA) for exchange–correlation potential, the projector augmented wave (PAW) method,^{50,51} and a plane-wave basis set with an energy cut off of 450 eV. All calculations were performed by sampling the gamma point of the Brillouin zone, and without using spin-polarization. The zero-damping DFT-D3 method of Grimme,⁵² was used for dispersion correction. The adsorbed molecules were fully relaxed until the net force on each atom was less than 0.01 eV Å⁻¹.

Localized DFT calculations for the pairwise interactions and electrostatic potential (ESP) maps were performed using Gaussian 16⁵³ with the B3LYP functional and 6-31G(d,p) basis set. The standard convergence criteria of the Gaussian 16 program were used for optimizations. Images of the simulated structures were generated using VESTA software.⁵⁴

MC simulations of TBTANG ordering were performed on a triangular lattice with periodic boundary conditions using the Metropolis algorithm and Kawasaki dynamics,⁵⁵ where the movement of molecules was simulated for a fixed value of molecular coverage of 0.1 mol/a². We used a slightly lower molecular coverage than that of the ideal Br...O phase to avoid a significant slowing down of the Kawasaki dynamics. A randomly selected molecule was allowed to jump into an unoccupied lattice site and change its orientation by rotation over 60 degrees (two molecular states). Movement was accepted with a probability $\exp(-\Delta E/kT)$, where ΔE is the energy difference between the final and the initial state of the system. Here T and k denote the temperature and the Boltzmann constant,

respectively. 10^7 MC steps per lattice site were performed to ensure a proper equilibration at each temperature.

Author contributions

F. D. M. and G. G. wrote the paper, and, together with M. C. G., participated in all experimental measurements and data analysis; M. S. and E. E. T. performed and analyzed the MC calculations; E. H., R. M. R. and Y. C. synthesized the molecules; D. D. participated in STM and XPS data acquisition and analysis; G. C. participated in XPS data acquisition and analysis; M. E. performed the DFT calculation and supervised the STM experiments; O. M. produced the ESP maps; M. C. G., F. R. and D. F. P. conceived the experiments and supervised the work; all authors participated in writing and editing the manuscript.

Conflicts of interest

There are no conflicts to declare.

Acknowledgements

This work was partially supported by a project Grande Rilevanza Italy-Quebec of the Italian Ministero degli Affari Esteri e della Cooperazione Internazionale (MAECI), Direzione Generale per la Promozione del Sistema Paese. The authors acknowledge funding from the Natural Sciences and Engineering Research Council of Canada (NSERC) and the Fonds Québécois de la Recherche sur la Nature et les Technologies (FQRNT) through a Team Grant. F. R. is grateful to the Canada Research Program for funding and partial salary support. D. F. P. thanks the US Army Office for Scientific Research and FQRNT-Team grant for partial support. Computations were performed mostly on the TCS and Niagara supercomputers at the SciNet HPC Consortium,^{56,57} funded by the Canada Foundation for Innovation under Compute Canada, the Government of Ontario, Ontario Research Fund – Research Excellence, and the University of Toronto. The simulations were also enabled by support from the Shared Hierarchical Academic Research Computing Network (SHARCNET: www.sharcnet.ca), WestGrid (www.westgrid.ca), and Compute Canada (www.compute-canada.ca).

References

- G. M. Whitesides and B. Grzybowski, *Science*, 2002, **295**, 2418–2421.
- G. M. Whitesides, J. P. Mathias and C. T. Seto, *Science*, 1991, **254**, 1312–1319.
- J. V. Barth, *Annu. Rev. Phys. Chem.*, 2007, **58**, 375–407.
- F. Cicoira, C. Santato and F. Rosei, *Top. Curr. Chem.*, 2008, **285**, 203.
- J. Puigmartí-Luis, A. Minoia, H. Uji-i, C. Rovira, J. Cornil, S. De Feyter, R. Lazzaroni and D. B. Amabilino, *J. Am. Chem. Soc.*, 2006, **128**, 12602–12603.
- T. Zhang, Z. Cheng, Y. Wang, Z. Li, C. Wang, Y. Li and Y. Fang, *Nano Lett.*, 2010, **10**, 4738–4741.
- G. M. Scheuermann, L. Rumi, P. Steurer, W. Bannwarth and R. Mülhaupt, *J. Am. Chem. Soc.*, 2009, **131**, 8262–8270.
- M. Pumera, *Energy Environ. Sci.*, 2011, **4**, 668–674.
- F. Rosei, M. Schunack, Y. Naitoh, P. Jiang, A. Gourdon, E. Laegsgaard, I. Stensgaard, C. Joachim and F. Besenbacher, *Prog. Surf. Sci.*, 2003, **71**, 95–146.
- C.-A. Palma, M. Cecchini and P. Samorì, *Chem. Soc. Rev.*, 2012, **41**, 3713–3730.
- S. Conti and M. Cecchini, *Phys. Chem. Chem. Phys.*, 2016, **18**, 31480–31493.
- M. O. Blunt, J. Adisoejoso, K. Tahara, K. Katayama, M. Van der Auweraer, Y. Tobe and S. De Feyter, *J. Am. Chem. Soc.*, 2013, **135**, 12068–12075.
- A. Ciesielski, P. J. Szabelski, W. Rzyśko, A. Cadeddu, T. R. Cook, P. J. Stang and P. Samorì, *J. Am. Chem. Soc.*, 2013, **135**, 6942–6950.
- F. De Marchi, G. Galeotti, M. Simenas, P. Ji, L. Chi, E. E. Tornau, A. Pezzella, J. MacLeod, M. Ebrahimi and F. Rosei, *Nanoscale*, 2019, **11**, 5422–5428.
- R. Gatti, J. M. MacLeod, J. A. Lipton-Duffin, A. G. Moiseev, D. F. Perepichka and F. Rosei, *J. Phys. Chem. C*, 2014, **118**, 25505–25516.
- K. G. Nath, O. Ivasenko, J. M. MacLeod, J. A. Miwa, J. D. Wuest, A. Nanci, D. F. Perepichka and F. Rosei, *J. Phys. Chem. C*, 2007, **111**, 16996–17007.
- M. Lackinger, S. Griessl, W. M. Heckl, M. Hietschold and G. W. Flynn, *Langmuir*, 2005, **21**, 4984–4988.
- B. Baris, V. Luzet, E. Duverger, P. Sonnet, F. Palmino and F. Cherioux, *Angew. Chem., Int. Ed.*, 2011, **50**, 4094–4098.
- L. C. Gilday, S. W. Robinson, T. A. Barendt, M. J. Langton, B. R. Mullaney and P. D. Beer, *Chem. Rev.*, 2015, **115**, 7118–7195.
- G. Cavallo, P. Metrangolo, R. Milani, T. Pilati, A. Priimagi, G. Resnati and G. Terraneo, *Chem. Rev.*, 2016, **116**, 2478–2601.
- R. Gutzler, O. Ivasenko, C. Fu, J. L. Brusso, F. Rosei and D. F. Perepichka, *Chem. Commun.*, 2011, **47**, 9453–9455.
- T. T. T. Bui, S. Dahaoui, C. Lecomte, G. R. Desiraju and E. Espinosa, *Angew. Chem., Int. Ed.*, 2009, **48**, 3838–3841.
- T. Clark, M. Hennemann, J. S. Murray and P. Politzer, *J. Mol. Model.*, 2007, **13**, 291–296.
- L. Grill, M. Dyer, L. Lafferentz, M. Persson, M. V. Peters and S. Hecht, *Nat. Nanotechnol.*, 2007, **2**, 687–691.
- D. F. Perepichka and F. Rosei, *Science*, 2009, **323**, 216–217.
- M. O. Blunt, J. C. Russell, N. R. Champness and P. H. Beton, *Chem. Commun.*, 2010, **46**, 7157–7159.
- G. Galeotti, F. De Marchi, T. Taerum, L. V. Besteiro, M. El Garah, J. Lipton-Duffin, M. Ebrahimi, D. F. Perepichka and F. Rosei, *Chem. Sci.*, 2019, **10**, 5167–5175.
- G. Galeotti, M. Di Giovannantonio, J. Lipton-Duffin, M. Ebrahimi, S. Tebi, A. Verdini, L. Floreano, Y. Fagot-

- Revurat, D. Perepichka, F. Rosei and G. Contini, *Faraday Discuss.*, 2017, **204**, 453–469.
- 29 S. Schlögl, W. M. Heckl and M. Lackinger, *Surf. Sci.*, 2012, **606**, 999–1004.
- 30 M. Bieri, M. T. Nguyen, O. Groning, J. M. Cai, M. Treier, K. Ait-Mansour, P. Ruffieux, C. A. Pignedoli, D. Passerone, M. Kastler, K. Mullen and R. Fasel, *J. Am. Chem. Soc.*, 2010, **132**, 16669–16676.
- 31 L. Lafferentz, V. Eberhardt, C. Dri, C. Africh, G. Comelli, F. Esch, S. Hecht and L. Grill, *Nat. Chem.*, 2012, **4**, 215–220.
- 32 J. Eichhorn, D. Nieckarz, O. Ochs, D. Samanta, M. Schmittel, P. J. Szabelski and M. Lackinger, *ACS Nano*, 2014, **8**, 7880–7889.
- 33 M. Di Giovannantonio and G. Contini, *J. Phys.: Condens. Matter*, 2018, **30**, 093001.
- 34 A. Saywell, W. Greñ, G. Franc, A. Gourdon, X. Bouju and L. Grill, *J. Phys. Chem. C*, 2014, **118**, 1719–1728.
- 35 M. Bieri, S. Blankenburg, M. Kivala, C. A. Pignedoli, P. Ruffieux, K. Mullen and R. Fasel, *Chem. Commun.*, 2011, **47**, 10239–10241.
- 36 C. Steiner, J. Gebhardt, M. Ammon, Z. Yang, A. Heidenreich, N. Hammer, A. Görling, M. Kivala and S. Maier, *Nat. Commun.*, 2017, **8**, 14765.
- 37 C. Steiner, B. D. Gliemann, U. Meinhardt, M. Gurrath, B. Meyer, M. Kivala and S. Maier, *J. Phys. Chem. C*, 2015, **119**, 25945–25955.
- 38 B. Zhang, Y. Chen, Y. Ren, L.-Q. Xu, G. Liu, E.-T. Kang, C. Wang, C.-X. Zhu and K.-G. Neoh, *Chem. – Eur. J.*, 2013, **19**, 6265–6273.
- 39 R. Gutzler, L. Cardenas, J. Lipton-Duffin, M. El Garah, L. E. Dinca, C. E. Szakacs, C. Fu, M. Gallagher, M. Vondracek, M. Rybachuk, D. F. Perepichka and F. Rosei, *Nanoscale*, 2014, **6**, 2660–2668.
- 40 Q. Sun, L. Cai, H. Ma, C. Yuan and W. Xu, *ACS Nano*, 2016, **10**, 7023–7030.
- 41 T. A. Pham, F. Song, M.-T. Nguyen, Z. Li, F. Studener and M. Stöhr, *Chem. – Eur. J.*, 2016, **22**, 5937–5944.
- 42 P. Maksymovych, D. C. Sorescu and J. T. Yates, *Phys. Rev. Lett.*, 2006, **97**, 146103.
- 43 G. Galeotti, M. Ebrahimi, J. Lipton-Duffin, J. M. MacLeod, S. Rondeau-Gagne, J. F. Morin and F. Rosei, *Phys. Chem. Chem. Phys.*, 2017, **19**, 10602–10610.
- 44 M. Šimėnas and E. E. Tornau, *J. Chem. Phys.*, 2014, **141**, 054701.
- 45 S. Suzuki, A. Nagata, M. Kuratsu, M. Kozaki, R. Tanaka, D. Shiomi, K. Sugisaki, K. Toyota, K. Sato, T. Takui and K. Okada, *Angew. Chem., Int. Ed.*, 2012, **51**, 3193–3197.
- 46 I. Horcas, R. Fernandez, J. M. Gomez-Rodriguez, J. Colchero, J. Gomez-Herrero and A. M. Baro, *Rev. Sci. Instrum.*, 2007, **78**, 013705.
- 47 G. Kresse and J. Furthmüller, *Phys. Rev. B: Condens. Matter Mater. Phys.*, 1996, **54**, 11169–11186.
- 48 G. Kresse and J. Hafner, *Phys. Rev. B: Condens. Matter Mater. Phys.*, 1993, **47**, 558–561.
- 49 J. P. Perdew, M. Ernzerhof and K. Burke, *J. Chem. Phys.*, 1996, **105**, 9982–9985.
- 50 P. E. Blöchl, *Phys. Rev. B: Condens. Matter Mater. Phys.*, 1994, **50**, 17953–17979.
- 51 G. Kresse and D. Joubert, *Phys. Rev. B: Condens. Matter Mater. Phys.*, 1999, **59**, 1758–1775.
- 52 S. Grimme, J. Antony, S. Ehrlich and H. Krieg, *J. Chem. Phys.*, 2010, **132**, 154104.
- 53 M. J. Frisch, G. W. Trucks, H. B. Schlegel, G. E. Scuseria, M. A. Robb, J. R. Cheeseman, G. Scalmani, V. Barone, G. A. Petersson, H. Nakatsuji, X. Li, M. Caricato, A. V. Marenich, J. Bloino, B. G. Janesko, R. Gomperts, B. Mennucci, H. P. Hratchian, J. V. Ortiz, A. F. Izmaylov, J. L. Sonnenberg, D. Williams-Young, F. Ding, F. Lipparini, F. Egidi, J. Goings, B. Peng, A. Petrone, T. Henderson, D. Ranasinghe, V. G. Zakrzewski, J. Gao, N. Rega, G. Zheng, W. Liang, M. Hada, M. Ehara, K. Toyota, R. Fukuda, J. Hasegawa, M. Ishida, T. Nakajima, Y. Honda, O. Kitao, H. Nakai, T. Vreven, K. Throssell, J. A. Montgomery, Jr., J. E. Peralta, F. Ogliaro, M. J. Bearpark, J. J. Heyd, E. N. Brothers, K. N. Kudin, V. N. Staroverov, T. A. Keith, R. Kobayashi, J. Normand, K. Raghavachari, A. P. Rendell, J. C. Burant, S. S. Iyengar, J. Tomasi, M. Cossi, J. M. Millam, M. Klene, C. Adamo, R. Cammi, J. W. Ochterski, R. L. Martin, K. Morokuma, O. Farkas, J. B. Foresman and D. J. Fox, *Gaussian 16, Revision B.01*, Gaussian, Inc., Wallingford CT, 2016.
- 54 K. Momma and F. Izumi, *J. Appl. Crystallogr.*, 2011, **44**, 1272–1276.
- 55 D. P. Landau and K. Binder, *A guide to Monte Carlo simulations in statistical physics*, Cambridge university press, 2014.
- 56 M. Ponce, R. van Zon, S. Northrup, D. Gruner, J. Chen, F. Ertinaz, A. Fedoseev, L. Groer, F. Mao, B. C. Mundim, M. Nolte, J. Pinto, M. Saldarriaga, V. Slavnic, E. Spence, C.-H. Yu and W. R. Peltier, in *Proceedings of the Practice and Experience in Advanced Research Computing on Rise of the Machines (Learning)*, ACM, New York, NY, USA, 2019, pp. 34:1–34:8.
- 57 C. Loken, D. Gruner, L. Groer, R. Peltier, N. Bunn, M. Craig, T. Henriques, J. Dempsey, C.-H. Yu, J. Chen, L. J. Dursi, J. Chong, S. Northrup, J. Pinto, N. Knecht and R. V. Zon, *J. Phys.: Conf. Ser.*, 2010, **256**, 012026.